Journal of Materials Chemistry A

Accepted Manuscript

ROYAL SOCIETY OF CHEMISTRY

www.rsc.org/materialsA

Journal Name

ARTICLE

Graphene-based Janus Micromotors for Dynamic Removal of Pollutants

Received 00th January 20xx,
Accepted 00th January 20xx

DOI: 10.1039/x0xx00000x

www.rsc.org/

Jahir Orozco,[a] Luiza A. Mercante,[ab] Roberto Pol,[a] and Arben Merkoçi[ac*]

Persistent organic pollutants (POPs) are ubiquitous in the environment as a result of modern industrial processes. We present an effective POPs decontamination strategy based on their dynamic adsorption at the surface of reduced graphene oxide (rGO)-coated silica (SiO_2)-Pt Janus magnetic micromotors for their proper final disposition. While the motors rapidly move in a contaminated solution, the adsorption of POPs is efficiently taking place in a very short time. Characterization of the micromotors both from the materials and from the motion point of view was performed. Polybrominated diphenyl ethers (PBDEs) and 5-chloro-2-(2,4-dichlorophenoxy) phenol (triclosan) were chosen as model POPs and the removal of the contaminants efficiently achieved. rGO-coated micromotors demonstrated to have superior adsorbent properties respect to the concomitant GO-coated micromotors, static rGO-coated particles and dynamic silica micromotors counterparts. The extent of decontamination was studied upon number of micromotors, whose magnetic properties were used for their collection from environmental samples. The adsorption properties were kept for 4 cycles of micromotors reuse. The new rGO-coated SiO_2 functional material-based micromotors showed outstanding capabilities for removal of POPs and their further disposition, opening up new possibilities for the efficient environmental remediation of these hazardous compounds.

Introduction

Persistent organic pollutants (POPs) are one of the most troublesome hazardous compounds wide-spread in the environment as residual products of modern industrial processes, remaining in the environment for long time.[1] For instance, polybrominated diphenyl ethers (PBDEs) are commonly incorporated as flame-retardants into many products (plastics, electronics, textiles, furniture and carpets).[2] 5-chloro-2-(2,4-dichlorophenoxy) phenol (triclosan) is often added in personal care products (deodorants, toothpastes, soaps), clothing and trash bags as antibacterial of broad spectrum.[3] Concerns about the environmental impact of these POPs are derived from their widespread use and subsequent residual persistence that is inherent to their physicochemical properties, including high stability, resistance to degradation and lipid solubility.[4] In this context, attempts to develop novel methods not only for accurate detection but also for efficient remediation of POPs are worthy of being explored.

Micro/Nanomotors have shown to offer unprecedented potential for a broad range of (bio)chemical science and industrial applications.[5,6,7] For example, it has been demonstrated the motion of self-propelled micromotors promoted the enhancement of analyte reaction-diffusion and solution accelerated mixing with interest not only in biosensing,[8] but also in stirring-free water decontamination strategies.[9] The outstanding competences of micromotors for environmental remediation have been recently highlighted in some reviews.[10,11,12,] Not only tubular catalytically propelled motors[8,9,13,14] but also Janus particle-based micromotors have been used for decontamination of organic pollutants.[15–17] These Janus micromotors comprise a surface of two different faces, each one exhibiting different physicochemical properties. Commonly, one of the faces is responsible of the propulsion, being the other one functionalized (or not) able to perform a particular remedial task. Novel Janus micromotors based on silver exchanged-zeolite/Pt and Mg/TiO_2 have been proven for the effective and rapid elimination of chemical and biological threats.[14,16,17] Charcol/Pt Janus micromotors were also reported for the dynamic adsorption of a variety of pollutants ranging from heavy metals and nitroaromatic explosives to organophosphorous nerve agents and azo-dye compounds.[15] Graphene-wrapped Janus micromotors were used to elucidate the mechanism that governs their motion[19] and to study their motion upon the influence of an applied electric field, a chemical potential gradient and an external magnetic field.[20] Yet, this is the first exploration of graphene-

[a] Nanobioelectronics and Biosensor Group, Catalan Institute of Nanoscience and Nanotechnology (ICN2), CSIC and The Barcelona Institute of Science and Technology, Campus UAB, Bellaterra, 08193, Barcelona, Spain. E-mail: aben.merkoci@icn.cat
[b] National Laboratory for Nanotechnology in Agribusiness (LNNA), Embrapa Instrumentation, 13560-970, São Carlos, SP, Brazil.
[c] ICREA – Catalan Institution for Research and Advanced Studies, Barcelona, 08010, Spain.

Electronic Supplementary Information (ESI) available: Supporting videos, experimental section and additional results. See DOI: 10.1039/x0xx00000x

based micromotors for a dynamic environmental remediation process.

Graphene-based materials have properties that are being harnessed for pollutant enrichment. For example their chemical stability, reduced cytotoxicity, large surface area (low density), high hydrophobic surface, large delocalized π electrons and large scale production possibilities are being exploited in the adsorption of contaminants, including dyes, organic pollutants and even metals.[21–26] The use of graphene nanosheets for the adsorption of POPs in water has been recently explored.[25,27] Adsorption capacity strongly depends on the graphene available sites to link the organic pollutants, mostly through π-π stacking interactions, and on the graphene nanosheets homogeneous dispersity in aqueous media. Pollutants that lack such organic rings are out of the scope of the model remediation strategy studied here. While the variety of oxygen functionalities of graphene oxide (GO) such as hydroxyl, carboxyl, and epoxy groups provide the material with hydrophilicity, at the same time arrange for a weak π electron structure that result in a poor affinity for aromatic organic pollutants. Reduction of graphene oxide (forming rGO) is a procedure that allows for recovering the adsorption capabilities of GO by giving back its hydrophobic character and π delocalized electron structure. Nevertheless, rGO nanosheets trend to aggregate due to large-area π-π interactions and strong van der Waals interactions between the graphene layers, thereby reducing the number of potential adsorption sites of graphene.[28] Loading rGO nanosheets onto low-cost substrates/carriers is a promising alternative to overcome such undesirable aggregation. Cheap, innocuous and abundant silica (SiO_2) is an ideal framework material to support rGO nanosheets preventing their aggregation. Accordingly, adsorption capabilities of rGO-coated SiO_2 composite materials (SiO_2@rGO) are worthy of interrogation for the efficient POPs remediation.

Herein, we present a rapid and efficient POPs decontamination strategy based on adsorption of the POPs at the surface of SiO_2@rGO-Pt Janus micromotors. The Janus micromotors are made up of a catalytic Pt layer hemisphere placed at a silica-graphene core-shell-like magnetic microparticle. While the Pt face efficiently self-propels the motors in a POPs contaminated solution the adsorption of these hazard compounds is efficiently taken place at their rGO face in a very short time. The as-prepared micromotors were characterized in terms of materials and motion. PBDEs[2] and triclosan[3] were chosen as model POPs and a polluted solution were efficiently decontaminated by the micromotors. The reduced graphene coated-micromotors demonstrated to have superior adsorption capabilities than their homologous static and dynamic counterparts. Effect of number of motors on the decontamination extend, adsorption and kinetic parameters were also determined. The fact of having the graphene adsorption sites fully expressed at the surface of a cheap, innocuous and magnetic silica-based substrate offers the possibility not only of an efficient POPs removal process but also of their easy collection from an environmental matrix by applying a magnetic field. The new SiO_2@rGO functional material-based micromotor demonstrated outstanding capabilities for POPs removal, which open up new possibilities for dynamic environmental remediation.

Results and Discussion

The Janus micromotor consists of two-dimensional rGO nanometric layers/flakes stabilized at a three-dimensional SiO_2 micrometric nontoxic structure and a hemispheric Pt thin layer used for POPs adsorption and micromotor propulsion, respectively. The microparticle substrate comprises some γ-Fe_2O_3 nanoparticles-containing an NH_2-SiO_2 core, with a spherical shape of 5.6 ± 0.8 µm average size, prepared as reported previously.[29] The micromotors fabrication process is presented in Figure 1A and detailed in both the S.I. Experimental Section and Figure S1. Figure 1A shows a sketch of the steps involved in the fabrication process, which comprises the coating of the silica core with a GO layer (1), reduction of the resulting GO-coated microparticle (2) and final recovering of the as-prepared rGO-coated silica particle with a Pt catalytic layer (3). Loading of GO onto the microparticles is achieved through electrostatic interactions coming from the opposite charge of NH_2-SiO_2 substrate and GO nanosheets at neutral pH, as confirmed by Zeta potential analysis (Figure S2). Posterior reduction of the GO-coated microparticles is chemically achieved with the environmental friendly ascorbic acid-based method, following a procedure reported in the literature.[30,31] Such reduction imposes again a hydrophobic character to the coating that allows for recovering the π electron structure, while keeping their adsorption places completely exposed at the whole surface.[25]

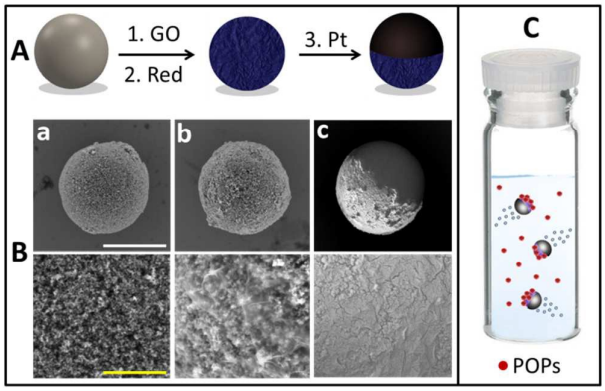

Figure 1. Micromotors fabrication process and POPs removal concept. A) Sketch of the steps involved in the fabrication process: 1) coating of a silica particle with graphene oxide (GO), 2) reduction of the GO-coated microparticles, 3) covering of half of the resulting rGO-coated silica particle with a Pt catalytic layer. B) Backscattered scanning electron microscopy (SEM) images of: a) a silica particle, b) a rGO monolayer-coated silica particle and c) a half covered Pt rGO-coated silica micromotor. Scale bars are 4 µm (upper line), 500 nm (bottom line). C) Sketch of the decontamination process: some Janus micromotors propelled in a POP solution.

The reduction will improve the adsorption capabilities of the coating, as will be demonstrated later in the removal experiments. rGO-coated SiO_2 microparticles were turned into microengines by covering the upper part of their surface (half part of the particle exposed to the coating process) with a 60 nm hemispheric Pt catalytic layer. Current intensity, which define the deposition rate, and thickness of the layer were tuned to get optimal motion of the micromotors (see details in the S.I. Experimental Section).

The superior adsorption capabilities of rGO are promoted by the micromotor motion in a contaminated solution, which results in an enhanced POPs removal capacity. Furthermore, the γ-Fe_2O_3 nanoparticles render the motors magnetic properties that offer the possibility of their complete collection from a sample after the POPs adsorption process. Zeta-potential of the particles were measured during the different steps of the fabrication process to trace the surface charge changes involved (Figure S2). An initial NH_2-SiO_2 surface charge of +16.9 ± 0.3 mV (due to the coating amino groups) was reversed to -41.4 ± 1.2 mV after GO self-assembly, indicating the negative charges from the GO sheets are predominating on the resulting particle surface. However, after the microparticle reduction process the zeta potential changed to -28.4 ± 0.4 mV. Such negative charge indicates that chemical reduction cannot fully eliminate the oxygen moieties and SiO_2@rGO microparticles still contain some residual oxygen functional groups. After the Pt-half covering the negative charge slightly shifted to -22.8 ± 1.6 mV, demonstrating that such Pt covering has only a little effect on the resultant micromotor electrical character. Topology of the particles was studied in the different steps of the fabrication process by scanning electron microscopy (SEM). Figure 1Ba shows the backscattered electron SEM image of a NH_2-SiO_2 microparticle rough surface, with no apparent difference respect its homologous rGO monolayer-coated SiO_2 one (Figure 1Bb). However, in the high-resolution SEM images (Figure 1Ba and b, bottom part) a clear difference in topography is observed. While the NH_2-SiO_2 (a) has a homogeneously distributed roughness, the rGO-coated SiO_2 microparticle surface (b) shows corrugated and scrolled nanosheets that resemble with some crumples. These closed-up images evidence the GO nanosheets where successfully assembled at the silica substrate (through electrostatic interactions as expected). Figure 1Bc shows a rGO-coated SiO_2 micromotor half-covered with Pt. The fact that around half of the surface appears brighter is an indication of the successful Janus micromotor fabrication process. Heavier elements (Pt) backscatter electrons more strongly than light elements (C, O), thus contrasting two well-defined areas of the particle with different chemical composition. The zoomed-in image (Figure 1Bc, bottom part) shows the cracked surface of Pt deposited at the top of the rGO-coated SiO_2 microparticle, necessary for the Janus micromotor propulsion. Figure 1C depicts a sketch of the decontamination process strategy, achieved by means of Janus micromotors propelled in a POP solution, where quantification of the amount of POPs after and before the removal process allows for estimation of the decontamination extent.

Figure 2A shows the energy-dispersive X-ray (EDX) spectroscopy images illustrating the distribution of the Si, O, Fe and Pt elements in the γ-Fe_2O_3 nanoparticles-containing SiO_2 inner core and the Pt catalytic patch, respectively. To

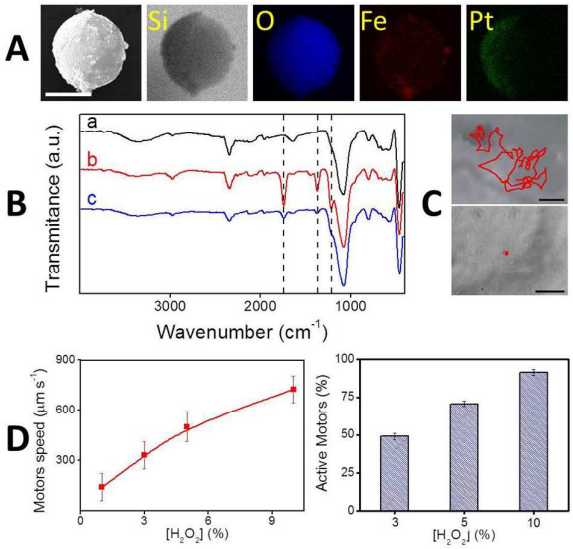

Figure 2. Characterization of the micromotors chemical composition and motion. A) Energy-dispersive X-ray (EDX) spectroscopy images illustrating the distribution of the Si, O, Fe and Pt elements in the γ-Fe_2O_3 nanoparticles-containing SiO_2 inner core and Pt catalytic patch, respectively. B) Fourier transform infrared (FTIR) absorption spectrum giving information about the chemical composition of GO (b) and rGO (c) coated SiO_2 microparticles, respect to the concomitant bare SiO_2 counterparts (a). C) Time-lapse images, taken from S.I video 1, of a Janus micromotor moving in the presence (upper part) and displaying Brownian motion in the absence (bottom part) of fuel for 7s, respectively. D) Micromotors speed dependence on the H_2O_2 fuel concentration (left) and number of micromotors (respect to the total) that remain active (reactive to H_2O_2) after the fabrication process (right). Error bars indicate the standard deviation of 20 measurements. Scale bar is 4 μm in A and 50 μm in C.

better understand the chemical composition of the particles coating (GO or rGO), Fourier transform infrared spectroscopy (FTIR) studies were further performed (Figure 2B). Loading of the NH_2-SiO_2 particles with GO and their posterior reduction led to a clearly differenced FTIR spectra that reflects the different chemical composition of the particles surface. For instance, the broad band between 3200–3400 cm^{-1} and the peak at 1638 cm^{-1}, attributed to -OH and O-H stretching vibrations,[32] respectively are prominent in the NH_2-SiO_2 particles (a), and decreased as GO sheets where assembled at the microparticles (b) and further reduced (c). The peak at 1735 cm^{-1} characteristic of C=O in carboxylic acids is absent in the particles spectrum (a) and higher in the GO-coated microparticles (b) respect to the rGO-coated ones (c). In the same fashion, other peaks such as those at 1211 and 1372 cm^{-1} characteristics of epoxy C-O and carboxyl O=C-O stretching vibrations, respectively do not appear in (a), while are higher in (b) respect to (c).[33] Overall, the decrease in number and intensity of the peaks in rGO-coated particles (c) respect to the corresponding GO-coated ones (b) indicate that the reduction process is eliminating many oxygen-containing groups, despite they are not completely eradicated from the surface. The peaks at 1080 and 450 cm^{-1}, related with Si-O-Si and Fe-O

stretching vibrations, respectively are consistent in the three spectra due to the common γ-Fe_2O_3-containing silica structure of the three different materials compared here. Micromotors were then characterized in terms of their motion. In the absence of H_2O_2 fuel, needed for micromotors propulsion, the SiO_2@rGO-Pt micromotors (Video S1, right side) display little random walks due to Brownian motion. However, in the presence of H_2O_2 fuel (Video S1, left side) the Pt catalytic surface of SiO_2@rGO-Pt promotes effective oxygen microbubbles evolution that generates a net momentum (directional thrust) that overcomes the Brownian motion, thus propelling the motor. Herein, sodium cholate (NaCh) is used as an anionic surfactant that, decreasing the surface tension, helps to modulate the size and frequency of the generated bubbles. Figure 2C (time-lapse image, upper part) shows the dramatic increase on the speed of a self-propelled SiO_2@rGO-Pt magnetic Janus micromotor in the presence of fuel, respect to the micromotor hardly moving with only Brownian motion in absence of it (Figure 2C, bottom part). Micromotors speed has shown to be very dependent on the H_2O_2 fuel concentrations (see details in S.I. Experimental Section). While the micromotor can move at an ultrafast speed of 725 ± 42 µm s^{-1} at 10 % H_2O_2 fuel concentration, they only move at 140 ± 15 µm s^{-1} at 1.5 % fuel concentration (Figure 2D, left). Video S2 shows the dramatic increase on micromotors speed upon increasing concentration of H_2O_2 fuel (up to 10 %). The driving force of the micromotors was calculated with the Stokes' drag expression for spherical colloids at low Reynolds number.[34] The Janus micromotors (at 10 % H_2O_2 fuel) achieve an ultrafast speed that corresponds to a large driving force of 33 pN, comparable with some previous Janus micromotor reports.[35] This driving force is amply sufficient to carry small chemical cargo such as PBDEs and triclosan, and even heavier cargo such as magnetic microparticles.[36,37] Both, speed and direction, are parameters to be controlled when micromotors are envisioned for real applications.[38,39] Herein, magnetic properties of the micromotors, essential to collect them from a sample after a POPs removal process, were also checked. Magnetic Janus micromotors were guided to the edge of a microdrop as a result of the application of a magnetic field from a magnet. When the magnetic field was off, the micromotors randomly migrated away from the microdrop edge (Video S3), thereby demonstrating the magnetic properties of the micromotors, coming from the γ-Fe_2O_3 nanoparticles of the micromotors inner core. Efficiency of the Janus micromotors catalytic hemisphere (for depletion of the H_2O_2 fuel) after the fabrication process was studied in terms of micromotors motion by estimating the number of motors that stay active in the presence of different concentrations of fuel, at 3% sodium cholate (NaCh) concentration (Figure 2D, right). Results show that although most of the micromotors vigorously produce bubbles, only up to 91% of the micromotors can move at 10% of H_2O_2 fuel concentration, while only around half of the population moves at 3% H_2O_2 fuel. This observation is an indication of the fact that along with the micromotor motion, bubbling is playing a key role in the diffusion of the pollutant towards the micromotors and further adsorption at their surface.[9] For example, the bubbles and fast micromotors movement have been shown to lead to enhanced mixing and acceleration of the mass transfer in bioafinity reactions,[40] to a motor-induced self-stirring in remediation experiments,[9] and to enhancement of the diffusion of passive tracers.[41] Overproduction of bubbles caused spilled sample container, thus having an adverse effect on the POPs adsorption process. Based on the aforementioned results, minimal fuel and surfactant concentrations down to 1.5 and 3% where selected as optimal conditions for the decontamination experiments, which resulted to be enough for an efficient removal of POPs, as demonstrated later.

A set of experiments was conducted to demonstrate the enhanced capabilities of the SiO_2@rGO-Pt Janus micromotors for removal of POPs. Quantification of the amount of POP after and before the micromotor-accelerated removal process was achieved by using the commercial Abraxis PBDEs and triclosan assays. The kits principle relies on a competitive assay where the target (each POP type) is competing with an enzyme-labelled homologous target for the binding sites at some POP-antibodies specific paramagnetic particles, following the scheme of an enzyme linked immunosorbent assay (ELISA).[42] Figure 3A shows the absorbance spectra of PBDEs (left) and triclosan (right) POPs removal experiments when 1 X 10^6 micromotors navigated in a 10 ppb contaminated solution for 10 min. The micromotor decontaminated solutions show spectra (dotted blue lines) which intensities are much higher than those from the contaminated ones (dashed red lines) and very close to those from the initial clean solutions (black continuous lines), respectively, as per the competitive immunoassay-based quantification method.

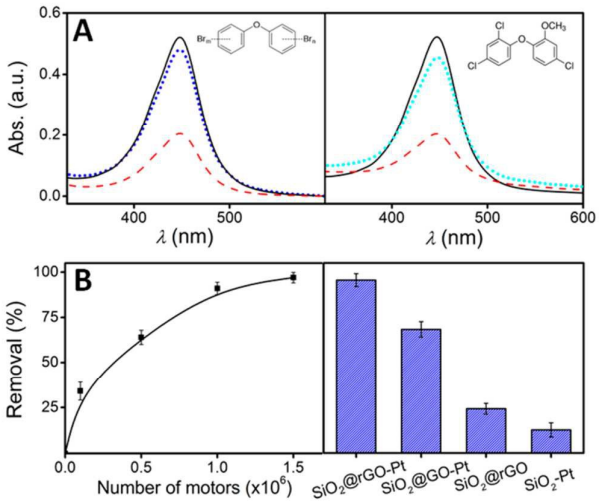

Figure 3. Micromotors-based removal of POPs. A) Absorbance spectra of the PBDEs (left) and triclosan (right) POPs: initial clean (continuous black line), contaminated (dashed red line) and decontaminated solutions (dotted blue line), respectively. B) Extent of decontamination upon number of motors (left) and comparison of the extent of decontamination (right) when using silica-coated reduced graphene oxide micromotors (SiO_2@rGO-Pt), respect to those obtained with silica-coated graphene oxide micromotors (SiO_2@GO-Pt), silica-coated reduced graphene oxide static microparticles (SiO_2@rGO) and silica micromotors (SiO_2@Pt), respectively. Error bars indicate the standard deviation of three measurements. Conditions: 500 µl of a 10 ppb POP contaminated solution containing, 1.5% H_2O_2, 3% NaCh and 1 X 10^6 micromotors.

From the spectra, the extent of removal was calculated to be 91.0 ± 3.4 and 87.0 ± 2.9 % for PBDEs (left) and triclosan

(right), respectively. These similar extents are consistent with the similar molecular structures of the POPs interrogated. The two aromatic rings, common in both structures, are the ones responsible of the π-π staking interactions with the rGO micromotors outermost surface cover. Further increase in the micromotors number can lead to both higher removal extents and/or adsorption of higher POPs concentrations. In this context, the extent of decontamination was studied upon the number of motors (Figure 3B, left side). When the amount of motors where increased up to 1.5 X 10^6, the extent of removal went up to 97.0 ± 2.9 %. These results demonstrated that the quantity of micromotors to be placed in a contaminated solution can be tailored depending on the grade of contamination of the sample and its volume.

The extent of PBDEs removal of SiO_2@rGO-Pt Janus micromotors were compared to those obtained with silica-coated graphene oxide micromotors (SiO_2@GO-Pt), silica-coated reduced graphene oxide static microparticles (SiO_2@rGO) and silica micromotors (SiO_2-Pt), respectively, when using the same micromotors number in the POP contaminated solution (Figure 3B, right). The enhanced adsorption achieved with the SiO_2@rGO-Pt Janus micromotors (91.0 ± 2.9 %) not only significantly decreased with the increase of oxygen groups in the outermost graphene nanosheets, *i.e.* the SiO_2@GO-Pt Janus micromotors (65.0 ± 4.1 %), but also dramatically decreased when the reduced graphene nanosheets-coated microparticles (SiO_2@rGO) where quiescent in the contaminated solution (23.0 ± 2.8 %). Remediation extent with only H_2O_2 was negligible, as expected. These results suggest that the superior adsorption capabilities and corresponding high extent of removal of POPs by the Janus micromotors are due to the synergistic effect of the highly hydrophobic character and the strong potential π-π stacking interactions of the exposed reduced graphene nanosheets,[25] combined with the enriched adsorption of the pollutants that is promoted by the enhanced mass transport from the micromotors motion.[15] In contrast, the SiO_2-Pt micromotors showed poor adsorption ability towards the POPs (12.0 ± 3.7 %), which is in agreement with their hydrophilic surface.[32]

To gain further insight into the adsorption mechanism, adsorption capacity of the micromotors (adsorbent) was then studied. The removal extent of PBDEs (adsorbate) is increasing upon time at the time range studied (1-10 min) and decreasing as concentration of PBDEs went from 5 (a), to 10 (b) and 20 (c) ppb, respectively, for the same amount of SiO_2@rGO-Pt Janus micromotors (Figure S3A). The mass of PBDEs adsorbed at the micromotors surface was estimated from the removal extend graph and Langmuir and Freundlich adsorption isotherms plotted at the system equilibrium state, t = 10 min. The Langmuir and Freundlich models are giving by the Equation 1 and 2, respectively. Where q_e is the amount of adsorbate per unit of adsorbent (mg g^{-1}), C_e is the adsorbate equilibrium concentration (mg l^{-1}), Q and b (Langmuir constants) and K_f and n (Freundlich constants) are related to adsorption capacity (Q and K_f) and rate of adsorption (b and n), respectively.

$$\frac{1}{q_e} = \frac{1}{Q} + \frac{1}{QbC_e} \qquad (1)$$

$$\ln q_e = \frac{1}{n}\ln C_e + \ln K_f \qquad (2)$$

When plotting $1/q_e$ *vs* $1/C_e$ (Langmuir) and ln q_e *vs* ln C_e (Freundlich) we found that the data fit slightly better the Freundlich isotherm model with a correlation coefficient R^2 of 0.9996, respect to 0.9982 from the Langmuir model. These results suggest that unlike uniform adsorption, the adsorption takes place on a heterogeneous surface at sites with different energy of adsorption. This is in agreement with the different graphene surface-energy adsorption sites, as compared to flatter surfaces.[25] From the fitted date, K_f and n were calculated to be 3.257 (mg g^{-1})(l mg^{-1})^n and 1.14, respectively. Such K_f value is much higher compared to that estimated from some NH_2-SiO_2 nanoparticles (0.0048), slightly higher respect to that from the particles decorated with some rGO nanosheets (1.7371) and much lower compared to only pristine graphene (149.26), as expected; all of them adsorbing phenanthrene POP at their corresponding static particle surface.[32] The n value, greater than unity, indicates that the PBDEs is favourably adsorbed at the SiO_2@rGO-Pt micromotors surface. The rate constant of adsorption was determined from the pseudo-first-order equation given by Langergren and Svenska (Equation 3) and from a pseudo-second-order equation based on equilibrium adsorption (Equation 4), respectively, where q_e is the sorption capacity at equilibrium and q_t is the loading of POP at time t. The parameters k_1 and k_2 (g (mg min)$^{-1}$) represents the pseudo-first- and pseudo-second-order rate constants for the kinetic models, respectively. The slope and intercept of the linear plots from Equantion 3 and 4 yield the values of q_e and k_2. The linear plots of ln q_e *vs* t and t/q_t *vs* t for 5 (a), 10 (b) and 20 (c) ppb, respectively show that data fit much better the pseudo-second-order kinetic model, indicating that chemisorption of PBDEs at the SiO_2@rGO-Pt micromotors surface is the rate determining step (see additional information in Figure S3B and Table S1). These results are in agreement with the kinetic model estimated for some POP at a GO adsorbent surface.[43]

$$\ln q_e = \ln (q_e - q_t) + k_1 t \qquad (3)$$

$$\frac{t}{q_t} = \frac{1}{K_2 q_e^2} + \left(\frac{1}{q_e}\right) t \qquad (4)$$

To test the effect of an environmental matrix on the removal process, towards demonstrating the practical utility of the SiO_2@rGO-Pt micromotors, we interrogated the removal extent of POPs in a seawater sample. Figure 4A (left side) shows the spectra of the PBDEs removal (dotted blue line), whose intensity is higher than that from the POP spiked - seawater sample (dashed red line), consistent with the competitive immunoassay used herein as quantification method, and closer to that from the initial unpolluted solution (black continuous line), respectively. From the spectra, the extent of removal was calculated to be 76 ± 2.8 %. The slightly lower extent, respect to that estimated from POP-spiked deionized water might be related with some matrix effects. π-π interactions between the rGO micromotors coating and some organic compounds that may eventually be present in the environmental sample might be accounting for such lower removal extent. Indeed, the micromotors speed in a contaminated solution containing 33% of seawater slows down to 100 ± 33 μm s^{-1} (Video S4). Such slower motion,

respect to the motion in a water sample (725 ± 42 μm s^{-1}), might be also accounting for the decrease in the removal extent. In a similar fashion, the extent of removal was also studied for a seawater sample where both PBDEs and triclosan are present. For this purpose a 5 ppb PBDEs and 5 ppb triclosan mixture were spiked in the seawater sample (Figure 4A, right side), and the extent of decontamination were calculated after the SiO_2@rGO-Pt micromotors-based accelerated removal. Quantification of PBDEs and triclosan in the mixture was separately achieved by using the corresponding kits (see S.I. Experimental Section). As both kits are based on the same immunodetection principle and they have shown to interfere with one another, we first estimated the effect of triclosan over PBDEs quantification and later the one of PBDEs over the triclosan quantification (see details in S.I Experimental Section). We found that when quantifying PBDEs in the presence of triclosan the concentration was overestimated in a 1.20 factor and when triclosan was quantified in the presence of PBDEs the concentration was overestimated in a 1.15 factor, in agreement with the literature.[42,44] The corresponding spectra were then normalized respect the empirically found factors when coexisting both POPs in the same seawater sample as shown in Figure 4A, right side. The doted blue and cyan lines are the normalized spectra for the removal of PBDEs coexisting with triclosan and vice versa, respectively respect to the spectra from the initial clean solution (continuous black line). The removal extents were estimated to be 74 ± 2.1 and 71 ± 3.2 %,

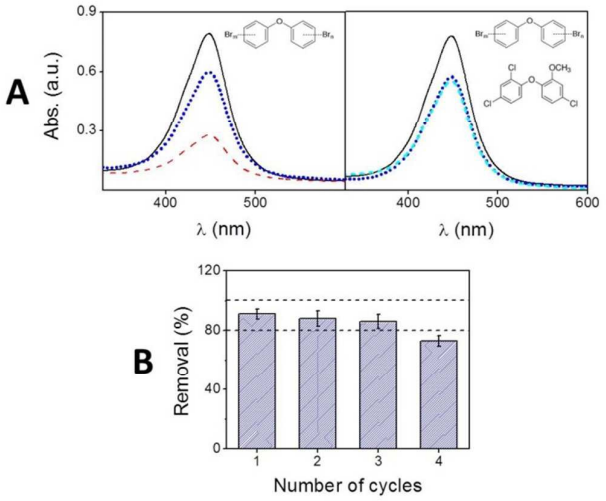

Figure 4. Removal of POPs in real environmental samples and micromotors reusability. Removal of POPs from a 10 ppb PBDEs (A, left side); and 5 ppb PBDEs and 5 ppb triclosan mixture in seawater contaminated solutions (A, right side), respectively. Initial concentration of spiked POP in the sample is in a dash red line, uncontaminated samples are in a black continuous line, removal of PBDEs and triclosan are in a doted blue line and a short dashed cyan line, respectively. B) Number of cycles that the same batch of micromotors was used for the removal of 10 ppb PBDEs. Error bars indicate the standard deviation of three measurements. Other conditions are as in Figure 3.

for PBDEs and triclosan, respectively. The removal extent of PBDEs when coexist with triclosan is quite similar to that obtained from PBDEs alone in the seawater sample and significantly lower when compared to that form deionized water. Yet, the removal extent can be potentially improved in real samples by slightly increasing the number of motors (Figure 3B, left) or the removal time (Figure S3A) depending on the concentration of POPs, as demonstrated for deionized water. These results indicate that adsorption capabilities of the micromotors towards the POPs are very promising for removal of these pollutants from real environmental samples and other contaminated samples. Therefore, such improved capabilities combined to the magnetic properties of the Janus micromotors can be exploited in the efficient adsorption of pollutants for their final disposal.

The ideal adsorbent material not only must have a high adsorption capability, but also should show desorption properties to be reused. Towards a practical application in water remediation, based on the micromotors adsorption capacity, we evaluated the recycling ability of the SiO_2@rGO-Pt micromotors while removing POPs. Pollutants adsorbed at porous graphene-based materials have been desorbed by heat, acidic and electric treatment, among other desorption methods.[43] However, those desorption methods may produce some further harming of the environment. One of the advantages of the moving adsorption platform proposed herein is its high stability from the structural and chemical point of view, which offers the possibility of regeneration cycles after each micromotors use by simply desorbing the adsorbed pollutants from them. Herein, reusability was studied based on the ± 3σ criterion. A control chart (Figure 4B) was plotted taking the mean value of the micromotor-based removal extent from successive measurements the first day of the study, considered as central value. The upper and lower control limits were set at three times the standard deviation of this value. The micromotor-based adsorbent platform was reused until the removal extent was lower than 3-folds the standard deviation of the removal measurements from the first cycle. Based on this criterion, the micromotors were reused for 4 cycles (Figure 4B) with a desorption step in between cycles performed in isooctane solvent as detailed in the S.I. Experimental Section. The micromotors magnetic properties were crucial not only for their magnetic separation in the reusability experiments, but also offers an alternative for the final disposition of the adsorbed pollutants after their removal from real environmental samples.

Conclusions

We have presented a SiO_2@rGO-Pt Janus micromotors-based strategy for the enhanced removal of PBDEs and triclosan POPs from environmental samples. These hazards pollutants were rapidly adsorbed at the outermost rGO coating from the micromotors while they were autonomously propelled in the contaminated solution. The reduced graphene coating demonstrated to have superior adsorption capabilities than its homologous graphene oxide form. In the same fashion, the dynamic adsorption of the POPs by the micromotors led to an enhanced removal extent when compared to the corresponding static counterparts. The synergistic effect of the superior adsorbent properties of the micromotor coating, along with the enhanced

adsorbate/adsorbent interaction -promoted by the micromotor motion- led to an improved removal extent of around 90% of POPs in only 10 min. The approach presented here can be explored in the decontamination of some other aromatic-containing pollutants whether conditions tailored by varying the number of micromotors based on the pollutants volume and concentration. The adsorption mechanism has shown to adjust better with the Freundlich model, following a pseudo-second-order kinetics, thereby indicating that chemisorption of POPs at the heterogeneous graphene-wrapped micromotors surface is the rate determining step. The magnetic properties of the micromotors were exploited to collect them from an environmental sample after the removal process. Successfully removal was achieved for 4 consecutive cycles. Overall, the new SiO_2@rGO functional material-based micromotor demonstrated outstanding capabilities for POPs removal, which open up new ways of dynamic environmental remediation of these troublesome hazardous compounds.

Acknowledgements

This work was supported by the European Commission Program, FP7-OCEAN, SMS Project (613844). ICN2 acknowledges support from the Severo Ochoa Program (MINECO, Grant SEV-2013-0295). Nanobiosensors and Bioelectronics Group acknowledges the support from Generalitat de Cataluña (Grant 2014 SGR 260). L.A.M acknowledges financial support from FAPESP-BEPE (2014/26088-4) project. D. Horák and B.A. Zasońska, from Institute of Macromolecular Chemistry (Czech Republic), are acknowledged for providing us with the SiO_2 microparticles. Authors also thank E. Morales for his wise advices.

References

1 K. Jones, P. De Voogt, *Environ. Pollut.*, 1999, **100**, 209.
2 A. Covaci, S. Harrad, M. A.-E. Abdallah, N. Ali, R. J. Law, D. Herzke, C. A. de Wit, *Environ. Int.*, 2011, **37**, 532.
3 G. S. Dhillon, S. Kaur, R. Pulicharla, S. K. Brar, M. Cledón, M. Verma, R. Y. Surampalli, *Int. J. Environ. Res. Public Health*, 2015, **12**, 5657.
4 M. S. El-Shahawi, A. Hamza, A. S. Bashammakh, W. T. Al-Saggaf, *Talanta*, 2010, **80**, 1587.
5 M. Guix, C. Mayorga-Martinez, A. Merkoçi, *Chem. Rev.*, 2014, **114**, 6285.
6 X. Lin, Z. Wu, Y. Wu, M. Xuan, Q. He, *Adv. Mater.*, 2015, 1.
7 J. Wang, Nanomachines: Fundamentals and Applications; Wiley-VCH: Weinheim, Germany, 2013.
8 E. Morales-Narváez, M. Guix, M. Medina-Sánchez, C. C. Mayorga-Martinez, A. Merkoçi, *Small*, 2014, **10**, 2542.
9 J. Orozco, G. Cheng, D. Vilela, S. Sattayasamitsathit, R. Vazquez-Duhalt, G. Valdés-Ramírez, O. S. Pak, A. Escarpa, C. Kan, J. Wang, *Angew. Chemie Int. Ed.*, 2013, **52**, 13276.
10 L. Soler, S. Sánchez, *Nanoscale*, 2014, **6**, 7175.
11 W. Gao, J. Wang, *ACS Nano*, 2014, **8**, 3170.
12 J. G. S. Moo, M. Pumera, *Chem. – A Eur. J.*, 2014, **21**, 58.
13 L. Soler, V. Magdanz, V. Fomin, S. Sánchez, O. Schmidt, *ACS Nano*, 2013, **7**, 9611.
14 J. Orozco, D. Vilela, G. Valdés-Ramírez, Y. Fedorak, A. Escarpa, R. Vazquez-Duhalt, J. Wang, *Chem. - A Eur. J.*, 2014, **20**, 2866.
15 B. Jurado-Sánchez, S. Sattayasamitsathit, W. Gao, L. Santos, Y. Fedorak, V. V. Singh, J. Orozco, M. Galarnyk, J. Wang, *Small*, 2015, **11**, 499.
16 V. V. Singh, B. Jurado-Sánchez, S. Sattayasamitsathit, J. Orozco, J. Li, M. Galarnyk, Y. Fedorak, J. Wang, *Adv. Funct. Mater.*, 2015, **25**, 2147.
17 J. Li, V. V Singh, S. Sattayasamitsathit, J. Orozco, K. Kaufmann, R. Dong, W. Gao, B. Jurado-Sánchez, Y. Fedorak, J. Wang, *ACS Nano*, 2014, **8**, 11118.
18 W. Gao, X. Feng, A. Pei, Y. Gu, J. Li, J. Wang, *Nanoscale*, 2013, **5**, 4696.
19 X. Ma, J. Katuri, Y. Zeng, Y. Zhao, S. Sánchez, *Small*, 2015, **11**, 5023.
20 S. Kumar, A. K. Singh, A. K. Dasmahapatra, T. K. Mandal, D. Bandyopadhyay, *Carbon*, 2015, **89**, 31.
21 S. M. Maliyekkal, T. S. Sreeprasad, D. Krishnan, S. Kouser, A. K. Mishra, U. V Waghmare, T. Pradeep, *Small*, 2013, **9**, 273.
22 E. Morales-Narváez, A.-R. Hassan, A. Merkoçi, *Angew. Chemie Int. Ed.*, 2013, **52**, 13779.
23 N. Ding, X. Chen, C. Wu, *Environ. Sci. Nano*, 2014, **1**, 55.
24 E. Morales-Narváez, T. Naghdi, E. Zor, A. Merkoçi, *Anal. Chem.*, 2015, **87**, 8573.
25 K. Yang, B. Chen, L. Zhu, *Sci. Rep.*, 2015, **5**, 11641.
26 G. Zhao, L. Jiang, Y. He, J. Li, H. Dong, X. Wang, W. Hu, *Adv. Mater.*, 2011, **23**, 3959.
27 Y. Shen, Q. Fang, B. Chen, Environ. Sci. Technol. 2015, **49**, 67.
28 F. Perreault, A. de Faria, M. Elimelech, *Chem. Soc. Rev.*, 2015, **44**, 5861.
29 P. Šálek, L. Korecká, D. Horák, E. Petrovský, J. Kovářová, R. Metelka, M. Čadková, Z. Bílková, *J. Mater. Chem.*, 2011, **21**, 14783.
30 J. Zhang, H. Yang, G. Shen, P. Cheng, J. Zhang, S. Guo, *Chem. Commun.*, 2010, **46**, 1112.
31 S. Eigler, S. Grimm, M. Enzelberger-Heim, P. Müller, A. Hirsch, *Chem. Commun.*, 2013, **49**, 7391.
32 K. Yang, J. Wang, B. Chen, *J. Mater. Chem. A* 2014, **2**, 18219.
33 X. Chen, B. Chen, *Environ. Sci. Technol.*, 2015, **49**, 6181.
34 E. Lauga, T. R. Powers, Reports Prog. Phys. 2009, **72**, 096601.
35 Y. Wu, Z. Wu, X. Lin, Q. He, J. Li, *ACS Nano*, 2012, **6**, 10910.
36 L. Baraban, M. Tasinkevych, M. Popescu, S. Sanchez, S. Dietrich, O. Schmidt, *Soft Matter*, 2012, **8**, 48.
37 L. Baraban, D. Makarov, I. Mönch, D. Grimm, S. Sanchez, O. G. Schmidt, *ACS Nano*, 2012, **6**, 3383.
38 L. Baraban, D. Makarov, O. G. Schmidt, G. Cuniberti, P. Leiderer, A. Erbe, *Nanoscale*, 2013, **5**, 1332.
39 J. Palacci, S. Sacanna, A. Vatchinsky, P. M. Chaikin, D. J. Pine, *J. Am. Chem. Soc.*, 2013, **135**, 15978.
40 D. Kagan, S. Campuzano, S. Balasubramanian, F. Kuralay, G.-U. Flechsig, J. Wang, *Nano Lett.*, 2011, **11**, 2083.
41 J. Orozco, B. Jurado-Sánchez, G. Wagner, W. Gao, R. Vazquez-Duhalt, S. Sattayasamitsathit, M. Galarnyk, A. Cortés, D. Saintillan, J. Wang, *Langmuir*, 2014, **30**, 5082.
42 W. Shelver, L. Kamp, J. Church, F. Rubio, *J. Agric. Food Chem.*, 2007, **55**, 3758.
43 H. Sun, L. Cao, L. Lu, *Nano Res.*, 2011, **4**, 550.
44 L. Kantiani, M. Farré, D. Asperger, F. Rubio, S. González, M. J. López de Alda, M. Petrović, W. L. Shelver, D. Barceló, *J. Hydrol.*, 2008, **361**, 1.

Table of Contents (ToC) Graphic

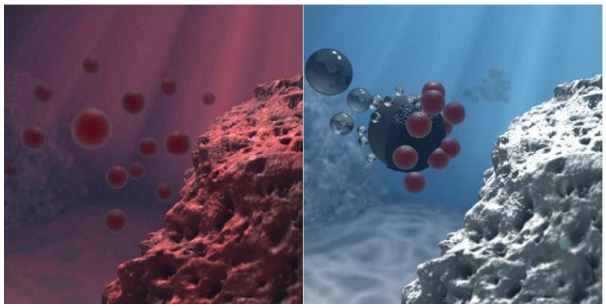

SiO_2@rGO-Pt Janus micromotors-based strategy for the enhanced removal of POPs for their proper final disposition.